Tanzania Journal of Engineering and Technology 2023, **42**(**3**): 114-128
OPEN ACCESS articles distributed under Creative Commons Attribution Licence [CC BY-ND]
Websites: https://ajol.org/tjet; https://tjet.udsm.ac.tz

ISSN 1821-536X (**print**); ISSN 2619-8789 (**electronic**)
https://doi.org/10.52339/tjet.v42i3.906

Regular Research Manuscript

Comparison of End-Point Energies of Bremsstrahlung Photons from 28-GHz ECR Ion Source in Three Measurement Locations

Mwingereza J. Kumwenda

Department of Physics, University of Dar es Salaam, Dar es salaam, TANZANIA

Corresponding author: kmwingereza@udsm.ac.tz, kmwingereza@yahoo.com

ORCID: https://orcid.org/0000-0003-1752-4807

ABSTRACT

Bremsstrahlung photons measurement show elevated energy emission beyond critical energy in 28-GHz ECR and its nature is not revealed. Thus, the aim of this study is to unveil the nature of high end-point energies at the three measurement locations. Bremsstrahlung photons from a 28-GHz ECR ion source were measured at Busan center of Korean Basic Science Institute (KBSI). The gamma-ray detection system consists of three round type NaI(Tl) scintillation detectors placed 62 cm radially from the beam axis at the three measurement locations namely injection, centre and extraction sides of an ECR ion source, and a NaI(Tl) scintillation detector placed at the view port for monitoring photon intensity along the beam axis. Such design of the experiment was based on the inner structure of the ECR ion source and the shape of the ECR plasma. Bremsstrahlung photons energy spectra were measured at RF power of 1 kW to extract O^{16} beam with a dominant fraction of O^{3+} and O^{4+}. Also, bremsstrahlung photons were measured by exchanging the detector positions for studying systematic uncertainties. Monte Carlo simulation based on the Geant4 package was performed to take geometrical acceptance and the energy-dependent detection efficiency into account due to large non-uniformity in the material budget. True bremsstrahlung energy spectra from the 28-GHz ECR ion source were extracted using an inverse matrix unfolding method. The measured high end-point energies at the three measurement locations were 1.68 MeV, 1.72 MeV and 2.04 MeV for the injection, centre and extraction sides, respectively. The high end-point energy values of the measured bremsstrahlung photons beyond the theoretical energy value of 1.33 MeV were found to be correlated with the structure of the ECR ion source and the shape of the ECR plasma. Furthermore, the high end-point energy values resulting from the bremsstrahlung photons measurements in the 28-GHz ECR plasma are due to the higher number of unconfined electrons arriving at the chamber wall easily, and producing higher bremsstrahlung photons. The unconfined electrons are the results of imperfect magnetic confinement that cause electrons to escape from the plasma volume. This study suggests a new design of magnetic confinement that will not allow an electron to escape.

ARTICLE INFO

First submitted: **Mar. 29, 2023**

Revised: **June 20, 2023**

Accepted: **Aug. 15, 2023**

Published: **Oct., 2023**

Keywords: *Bremsstrahlung photons, ECR ion source, RF power, NaI(TI) detectors, Unfolding*

INTRODUCTION

Electron cyclotron resonance ion sources (ECRIS) are used to produce multicharged ion beams extracted from a magnetized plasma taking advantage of accelerating electrons in a magnetic field with a GHz range radio frequency microwave (Thuillier *et al.*, 2022). The multiply charged ions are produced inside the plasma and confined with magnetic fields. Due to the unique capability of producing highly charged ion beams, the ECR ion sources are widely used in heavy ion accelerators and atomic physics research (Kasthurirangan *et al.*, 2012)**.** In the ECRIS electrons are heated resonantly by microwaves to provide ionization of neutral gases. During the bombardment of electrons, the ions or atoms are ionized, leading to charges up to the maximum charge with all electrons stripped off. A highly charged ion generates bremsstrahlung photons emission when it is decelerated or stopped in the materials (Leitner *et al.*, 2008; Ropponen *et al.*, 2009*).*

In the ECR ion source, two processes in the plasma lead to the emission of bremsstrahlung radiations. First bremsstrahlung is created by electron-ion collisions within the plasma volume. The second process is when electrons are lost from the plasma, collide with the plasma chamber wall, and radiate bremsstrahlung due to their sudden deceleration. The produced bremsstrahlung photons deposit energy in the structure of ion sources and turn out to be a substantial heat load to the cryostat in the case of superconducting ECR ion sources. The cryogenic system can remove only a limited amount of heat from the cryostat. If more heat is added to the system than it can be removed, then the temperature of the liquid helium rises and can cause the superconducting coils to quench (Leitner *et al.*, 2006; Benitez *et al.*, 2016).

Measurements of the bremsstrahlung photons produced in the ECRIS have been made since the late 1960s (Noland, 2011). However, many of these experiments attempt used to measure the bremsstrahlung photons in one direction either radially or axially, using one or two detectors but under different conditions. Nevertheless, the bremsstrahlung photons emitted from the ECRIS is expected to be anisotropic due to various effects (Noland, 2010; Bhaskar, 2021). Therefore, previous measurements of the bremsstrahlung photons were not enough to unveil possible causes of elevated energy components in the ECR ion source. It is very important to measure the angular distributions of the bremsstrahlung photons for a full dimension of the ECR ion source along the beam axis at the injection, centre, and extraction sides. This work saves of great importance as it is the first experimental work to measure, the emission of bremsstrahlung photons in azimuthal angular distributions from the 28-GHz ECR ion source plasma in six, three, and nine radial positions at the injection, centre, and extraction side respectively, using four thallium activated Sodium Iodine scintillation detectors. Three round-type NaI(Tl) detectors were used to measure the bremsstrahlung photons in the radial direction and one NaI(Tl) detector was placed in the axial direction for monitoring the intensity of the ECR plasma. Such design of the experiment was based on the inner structure of the ECR ion source and the shape of the ECR plasma. The ECR plasma is formed in the shape of a twisted triangular prism, due to hexapole fields. Therefore, the objective of this study is to compare the end-point energies of the bremsstrahlung photons emitted at the injection, centre, and extraction side and to unveil the nature of the elevated energy component of bremsstrahlung photons beyond a critical energy value suggested by the theory.

.

METHODS AND MATERIALS

Experiment Setup and Data Acquisition System

The bremsstrahlung photons data that were used in this study was measured from the 28-GHz superconducting ECR ion source of the compact linear accelerator facility at the Korea Basic Science Institute (KBSI), cyclotron research center. ECR ion source developed at KBSI is composed of six racetrack hexapole coils and three mirror solenoid magnets (Park *et al.,* 2014). The axial magnetic field is about 3.6 T at the beam injection area and 2.2 T at the extraction region, respectively. A radial magnetic field of 2.1 T can also be achieved on the plasma chamber wall. The cylindrical plasma chamber is 50 cm long and 15 cm in diameter, respectively. The chamber is made of stainless steel (SUS316L) and the chamber volume is kept at an ultra-high vacuum of 10^{-8} Torr (Lee *et al.,* 2012). The inner diameter of the hexapole coil is 207 mm from the beam axis and the coil thickness is 76 mm. NbTi superconducting wire was used for the magnet system. A higher current density NbTi wire was selected for winding of sextupole magnet. The inner face of the 49 mm thick solenoid coil is placed at a distance of 442 mm from the beam axis. The 50 mm thick iron shielding structure is 1200 mm wide, 1220 mm high, and 1700 mm long as shown in Figure 1 (Park *et al.,* 2016).

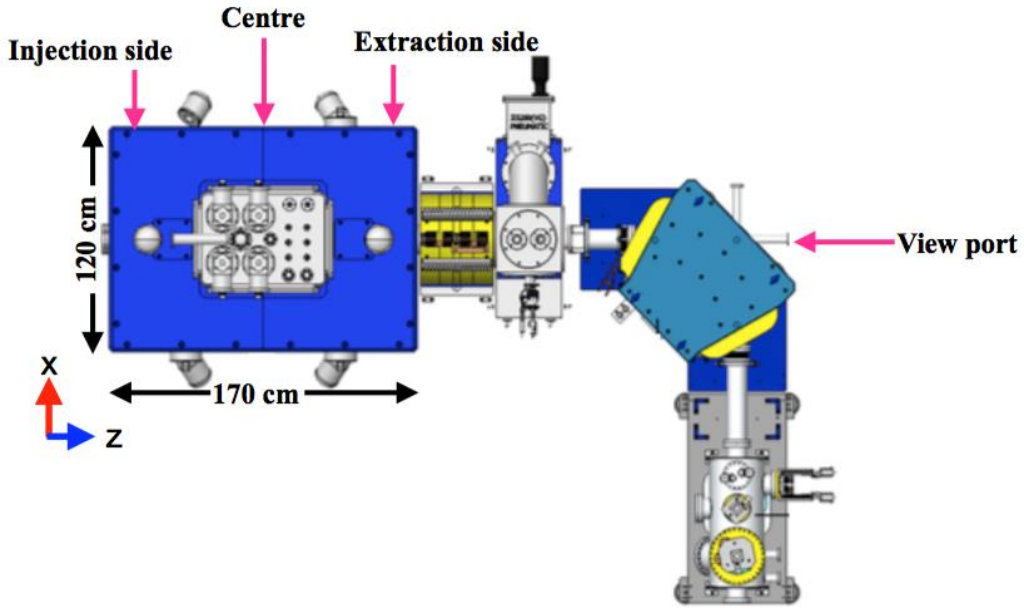

Figure 1: Schematic view of the low-energy accelerator facility at Busan Center of KBSI. A NaI(TI) detector is placed at the view port of bending magnet monitor.

This study has made use of four identical cylindrical NaI(TI) ORTEC 905-3 series detectors. The crystals are optically coupled to the PMT and encased in a light-tight aluminium case. The face of each detector had a diameter of about 5.08 cm (2 inches by 2 inches crystal size). The detectors are attached to pre-amplifiers for maintaining the time constant of the pulse. The average energy resolution of these detectors is about 7% for full width at half maximum (FWHM) at 662 keV. Each detector has 3 connectors at its rear, high voltage (HV), Anode and Dynode, which is damped by a 50-ohm resistor for this experiment. Both detectors are attached to the pre-amplifiers for maintaining the time constant of the pulse.

The experiment setup to measure bremsstrahlung photons spectra in this study was made different from the previous experiments conducted by other researchers. The inner structure of the ECR ion source and the shape of the ECR plasma

were considered in designing this experiment. Photon energy spectra were measured using three round type NaI(TI) detectors as shown in Figure 2 facing the edge of ECRIS. All detectors were labeled with letters D1, D2, D3, and D4 for easy reference, which were operated at +1300 V. The three detectors (D1, D2, and D3) were mounted on the support structure for radial measurements, as shown in Figure 2, while the D4 detector (Figure 1) was placed at the view port for monitoring the intensity of the ECR plasma.

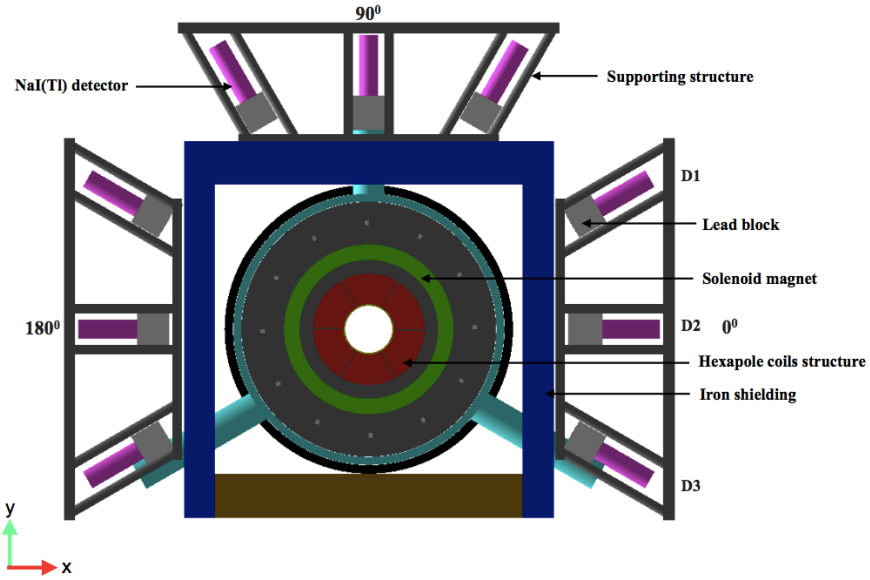

Figure 2: Schematic view of the nine NaI(Tl) detectors at the extraction side.

The bremsstrahlung photons were measured in six, three and nine azimuthal angles at the injection, centre and extraction sides of the ECR ion source. At first setup, the three round type NaI(Tl) detectors were placed at the three sides namely right, top and left as depicted in Figure 2 (for the extraction side). Thereafter, the detector system was moved to the centre (right position only) and lastly moved to the injection side (top and right position). The photon energy was measured at six, three and nine azimuthal angles in a 30° interval at the injection, centre and extraction sides respectively. The detector face was approximately 2 cm from the iron shielding structure. Each NaI(Tl) detector was placed in a Pb collimator of $100\times100\times100\ mm^3$ with a 5 mm hole. The Pb collimator covered a full dimension of the NaI(Tl) crystal.

NKFADC500 flash ADC which measures input pulse shape was used for data acquisition as illustrated in Figure 3. The detector signal was fed to the splitting module and then to a 500MHz FADC and recorded in a coincidence with a reference signal from the detector D4 placed at the view port. The 4-channel flash ADC module (Notice Co.) recorded full pulse information from four NaI(Tl) detectors in every 1μs. Typical pulse shapes are superimposed as in Figure 4. The ring-buffer data were then fed to a DAQ PC. Trigger logic OR provide event triggering condition. Due to the huge data size, the measurement was performed in every 180 seconds.

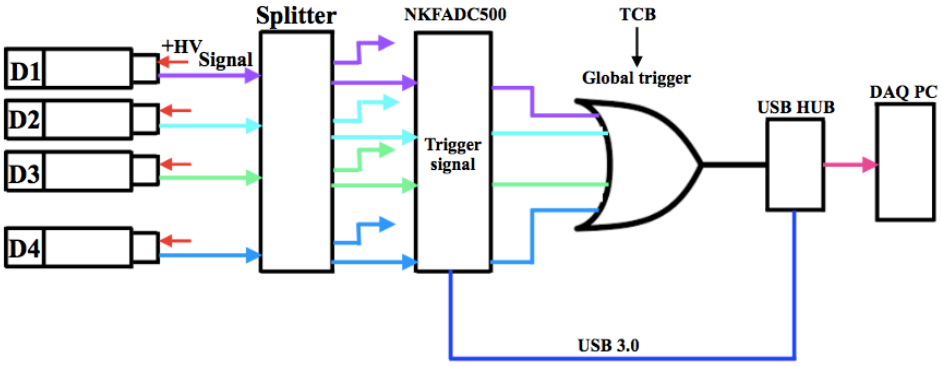

Figure 3: Schematic of an electronic data readout showing the signal from each detector.

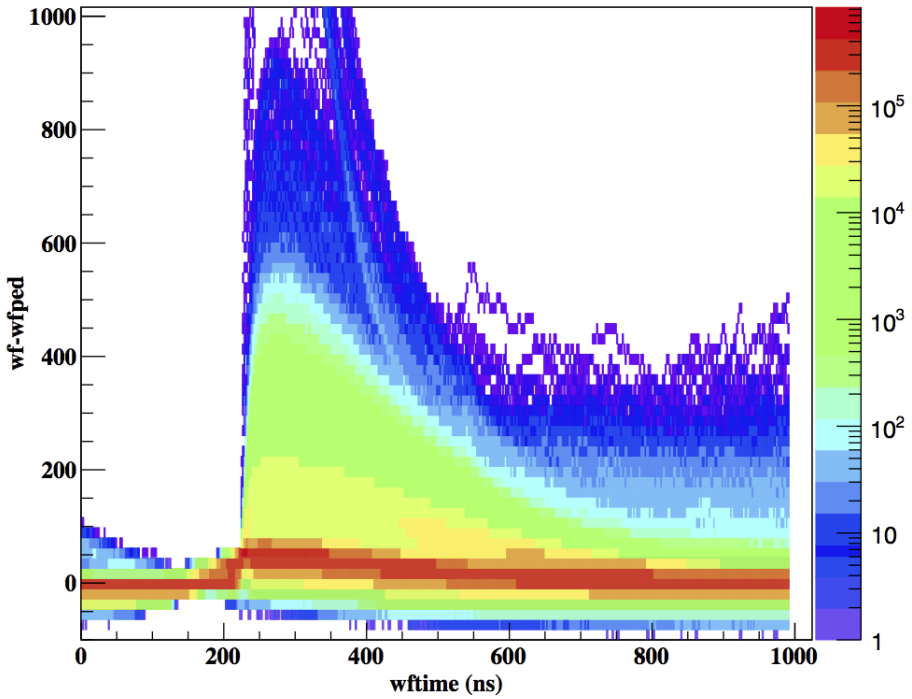

Figure 4: Superimposed NaI(Tl) detector signals digitized using a NKFADC500 (500-MHz flash ADC).

DATA ANALYSIS

Background and Energy Calibrations

During the measurement, the energy calibrations of the spectra were taken using standard radioactive gamma-ray's sources namely, ^{60}Co source with gamma-ray energies of 1173 keV and 1332 keV and ^{137}Cs source gamma-ray energy of 662 keV (Hajheidari, 2016). The three calibration data points were fitted with a linear straight line using a least-squared chi-square linear fit to convert each energy value to its corresponding channel. The background photon energy spectrum was measured for 10 hours and was normalized with the data taking time and subtracted from the raw spectra for bremsstrahlung photon measurement (the background event rate is 21 counts/s).

Direct Matrix Inversion Unfolding Method

The measured spectrum in the physical experiment is usually distorted and transformed by different detector effects, such as finite resolution, limited acceptance, efficiency variations, perturbations produced by the electronic

device, etc. In order to reproduce the true photon spectrum from the measured distributions it is necessary to consider these effects by means of response function (Benitez *et al.*, 2008; Thuillier *et al.*, 2022). Normally the response functions are obtained by the response matrix. From the basic mathematical relationship, the measured spectrum $M(E)$ can be given as follows:

$$M(E) = R(E, E_0)T(E_0) \quad (1)$$

Where $T(E_0)$ is the original or true energy distribution of the gamma rays emitted by the source and $R(E, E_0)$ is the matrix indicating the response function of the detector. The task is to obtain the true gamma-ray spectrum given the measured energy spectrum. Thus, the desired photon spectrum $T(E_0)$ is calculated from the matrix equation as follows;

$$T(E_0) = R^{-1}(E, E_0)M(E) \quad (2)$$

where $R^{-1}(E, E_0)$ is the inverse of the response matrix.

The pulse height distributions from various mono-energetic gamma-ray spectra were obtained from Monte Carlo simulation based on Geant4 package using "2 by 2 inches" NaI(Tl) scintillation detector.

Simulation of Response Function

In this study, the Monte Carlo method based on the Geant4 package codes was used for the formation of the response matrix. For the formation of the response matrix, one might need more than 100 spectra depending on the dimension of the problem one dealing with, which is very time-consuming and complicated work (Benitez *et al.*, 2008). To minimize the workload in making the response matrix, this study simulated 200 γ-ray's spectra ranging from 50 to 2040 keV with an interval of 10 keV as represented in Figure 5 in 2D. The z-axis of the 2D spectrum shows the peak-to-total ratios which gives the diagonal elements of the response matrix. The peak at 200 keV is due to the Compton backscattering as the result of the random direction of the gamma photons during simulation. The other peaks in the y-axis are single and double escape peaks when the gamma photons reach a threshold of 1.02 MeV (Kumwenda, 2018).

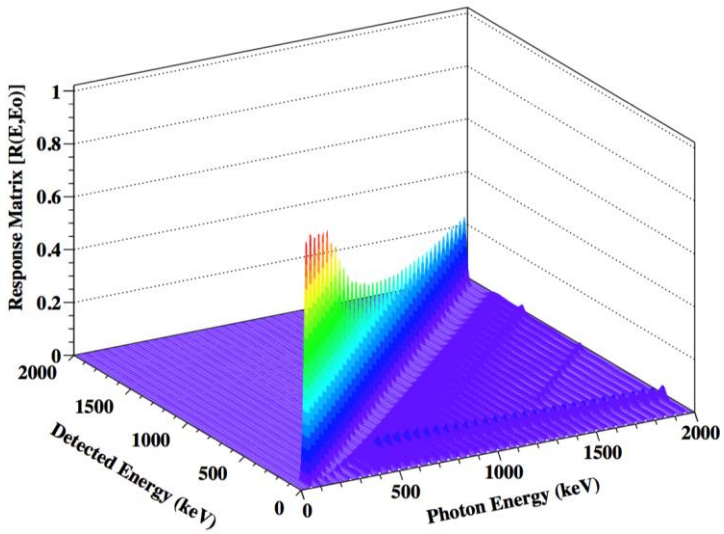

Figure 5: Simulated Response function from various mono-energetic gamma rays using NaI(Tl) scintillation detector in 2D.

To acquire reliable results, the simulated response function must be obtained with the same conditions as an actual experiment. For the accuracy of the unfolding method defined in equation (1), the response function $R(E, E_0)$ should have many energy

points (Benitez *et al.*, 2008). The validity of the simulated results was also checked by comparison of experimental and simulated spectra as displayed in Figure 6. The comparison of the measured and simulated spectra was done using a radioactive standard gamma source of ^{137}Cs.

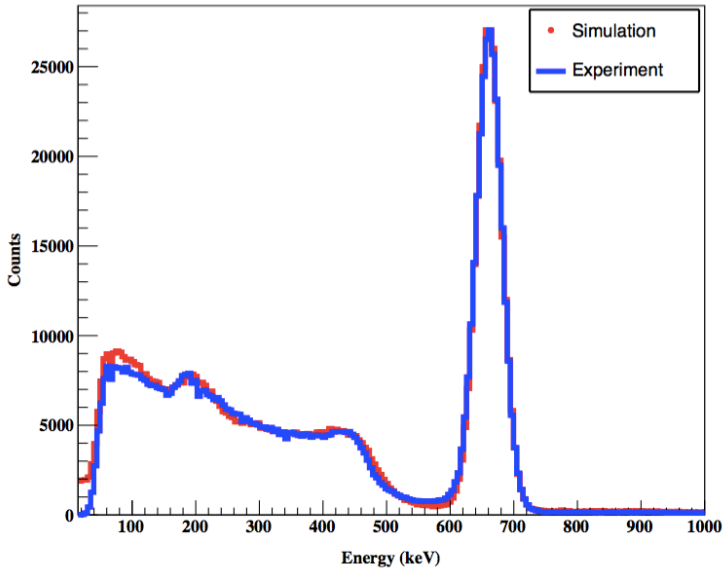

Figure 6: Comparison of experimental and simulated results using standard gamma-ray source.

It is clear from Figure 5 that, there is a good agreement between the simulated and measured spectra around the photo-peak region, but a slight deviation is observed below 0.2 MeV. The simulated and measured shows a peak at around 0.2 MeV that is caused by Compton backscattering. It is also observed that the simulated spectra show lower counts between Compton edge and photo-peak that might be caused by a single Gaussian function for broadening.

Peak to Total Ratio

In a mono-energetic gamma-ray radiation pulse height spectrum, the peak-to-total ratio is the number of counts contained in the total energy absorption to that contained in the whole spectrum. When a photon with energy E_0 is radiated there is a certain chance of being fully detected or partially detected. The probability that a photon of energy E_0 is detected with energy E is given by the response matrix $R(E, E_0)$. The response matrix gives the probability that a photon is detected. In order to obtain a response matrix $R(E, E_0)$ one needs to calculate the Peak-to-Total ratio (P/T) (Rahma and Cho, 2010; Almaz *et al.*, 2007). To obtain the peak-to-total ratio, the mono-energetic gamma spectrum peak was fitted to the Gaussian functions, and the peak region was calculated by taking 1.96σ value that makes 95% confidence level for the peak region. The peak region boundary was established as $(\mu - 1.96\sigma, \mu + 1.96\sigma)$ and counts under this region were divided by the total counts of the whole spectrum to get P/T which gives the diagonal elements of the response matrix. In order to fill in the remainder of $R(E, E_0)$ the P/T for each photon energy E_0 is subtracted from the unity and the remainder is shared equally in the energy region between zero and Compton edge. This is the maximum energy that can be absorbed due to Compton scattering which is given by equation (3).

$$E_c = \frac{2E_\gamma^2}{m_e c^2 + 2E_\gamma} \qquad (3)$$

where m_e is the mass of an electron and E_γ is the photon energy.

Unfolding Procedures

In practice, unfolding methods can be divided into two groups, direct and iterative. In this analysis, a brief description of the direct matrix inversion unfolding algorithm is presented. The algorithm is linear (no loops involved). The response matrices were arranged as a row and column to form M by M upper triangular response matrix. The obtained upper triangular matrices $M \times M$ were inverted using TMatrix class ($TMatrix :: kInvert$) in a ROOT programming language. To obtain vector $M(E)$, the measured spectrum was integrated in a 0.01 MeV energy interval. The multiplication of matrices R^{-1} and column vector M gives another column matrix T, which is the true gamma-ray spectrum of the detector. The acquired column vector T was filled in the histogram for plotting true energy spectrum from the measured spectrum. Also, the correctness of the response matrix was checked by multiplying R and R^{-1} and the results show that all elements along the diagonal are unity while in the inverse matrix, all elements above the diagonal are negative numbers. These are physically admissible. When the measured spectrum vector M is multiplied by the inverted matrix R^{-1}due to photons of a given energy the number of photons falls entirely in the channel corresponding to the given energy in the true spectrum for the mono-energetic spectrum (Figure 7). Since the diagonal elements are positive the above statement can be true only if all elements above the diagonal are negative (Kumwenda, 2020).

Validation of Unfolding Method

Multi-lines Sources (^{133}Cs and ^{60}Co)

Multi-lines and continuous energy spectra were used to check the reliability of the unfolding software, in this study Cobalt-60 which decay to Nickel-60 via beta-minus emissions is presented. The decay is initially to nuclear excited-state of Nickel-60 from which it emits either one or two gamma rays to reach a ground state of the Nickel-60 isotope (Be *et al.*, 2004). It is known that ^{60}Co has two gamma lines with almost the same probability of emission. However, the measured spectrum Figure 7(a) shows that the 1333 keV line populates much less than the lower line. By application unfolding matrix both two gamma lines of ^{60}Co (Figure 7(b)) show a similar probability of emission as it expected.

Strontium (^{90}Sr) Source

^{90}Sr source which emits bremsstrahlung photons was also used. ^{90}Sr which has a half-life of 28.8 years is a radioactive source which decay to Yttrium-90 with maximum energy of 546 keV. ^{90}Y in turn undergoes beta decay with half-life of 64 hours and maximum energy of 2300 keV to stable ^{90}Zr (Romero, 2012). ^{90}Sr generates electrons of a continuous energy spectrum, Figure 8 shows the corresponding beta spectrum of ^{90}Sr. To unfold ^{90}Sr, 230 γ-ray's spectra ranging from 0.05 to 2.35 MeV with an interval of 10 keV were simulated.

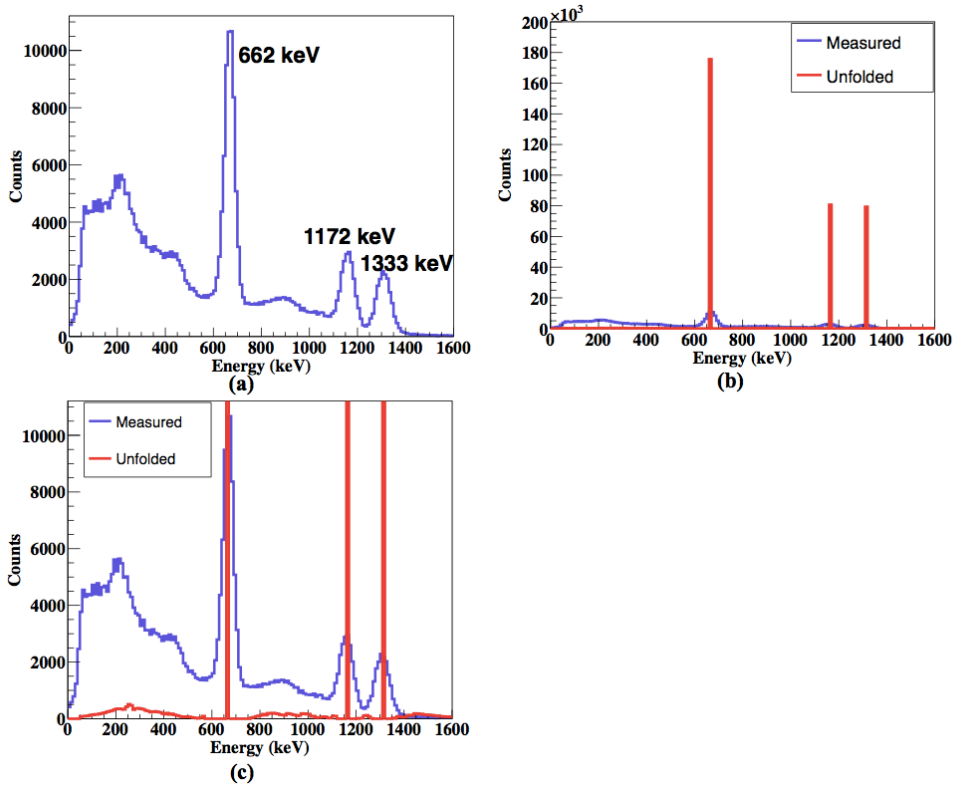

Figure 7: Measured energy spectrum of ^{60}Co and ^{137}Cs and unfolded spectrum (Red histogram) using the matrix inversion method.

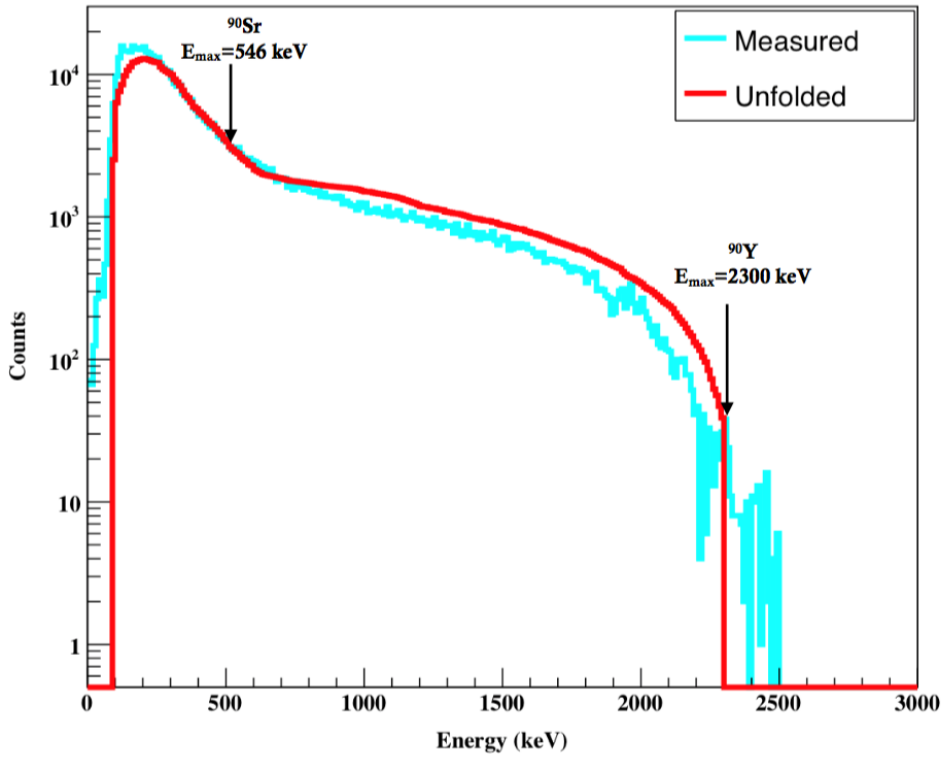

Figure 8: Measured spectrum of a ^{90}Sr source (Cyan) and unfolded spectrum (Red) using the matrix inversion method.

Bremsstrahlung Photons from ECR Ion Source

Energy Spectra of Bremsstrahlung Photons

Due to the complicated structure of the ECR ion source, the material budget differs largely depending on the azimuthal angles. The rectangular cross-section of the iron yoke structure and the racetrack sextupole coil structure give large non-uniformity in the material budget. In order to take the geometric acceptance and also the energy-dependent detection efficiency into account the Monte Carlo simulation based on the Geant4 package was performed. Thus, the measured energy spectra in the radial direction were corrected with the simulated efficiencies. Figure 9 shows the bremsstrahlung photon energy spectrum measured using the NaI(Tl) detector (D4) at the view port. The D4 detector was used to monitor a possible variation in the ECR plasma intensities throughout the measurements. All measured spectra in azimuthal angles were normalized to the number of events taken in the same time interval by the D4 detector.

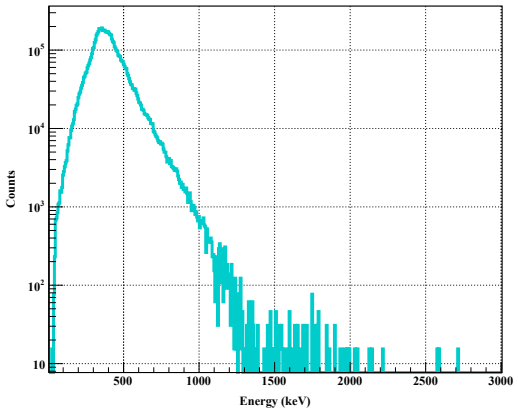

Figure 9: Measured energy spectrum of bremsstrahlung photons by the detectors D4.

The energy spectra for different azimuthal angles at the injection, centre, and extraction side of the ECR ion source were measured as shown in Figure 10(a, b, c). For the injection side, the slope in the high-energy tail indicates the characteristics of the source of the bremsstrahlung photons. The slope of the 90° energy spectrum is the same with 330° energy spectrum indicating that the spectra originate from the same source of bremsstrahlung photons. The energy spectra of bremsstrahlung photons at the extraction side of the ECR plasma for different azimuthal angles were measured using detector D1 as shown in Figure 10(c). The measured energy spectra depend highly on the azimuthal angles, in particular, yielding a significant difference in the low-energy region. The bump structures that appear near (0.2 - 0.3) MeV in both 10(b) and (c) are most likely caused by a combination of attenuation of photons through various materials in the source as well as cumulative Compton backscattering contribution associated with low-energy bremsstrahlung photons. The photon intensity changes drastically according to the azimuthal angles. The slope in the high-energy tail indicates the characteristics of the source of bremsstrahlung photons. The slope of the 330° energy spectrum (dark green histogram) is different from all others for all three detectors. Moreover, the 150° energy spectrum (black histogram) shows a long tail near 2 MeV, which is beyond the maximum kinetic energy available from ECR heating. The other two detectors at the extraction side show similar behaviour. Therefore, the two different slopes could originate from the different sources of the bremsstrahlung photons.

Unfolding of Bremsstrahlung Photons

The measured spectrum does not directly replicate the photons spectrum emitted by the electrons that reach the detector. There are several processes including attenuation and scattering that can alter the recorded spectrum before the photons are recorded in the data acquisition system. Therefore, correcting the detected spectra to get accurate spectra is very crucial in the attempt towards unveiling the nature of the elevated energy component of

bremsstrahlung photons from the ECR plasma. Thus, to obtain true bremsstrahlung photons spectra from measured ones, the direct matrix inversion unfolding method was applied as explained in the previous subsections. Figure 11 shows one of the results obtained when the bremsstrahlung photons spectrum was unfolded. The number of counts at the end of the high-energy region of the spectrum increase. During unfolding, the starting energy point was set to be 0.4 MeV due to fact that in a typical ECR ion source, the total material thickness in the radial direction is several tens of millimeters and consists of different elements. Due to the material thickness, the lower energy part of the bremsstrahlung spectrum is largely damped as the radiation penetrates the complicated structure. The threshold selection of 0.4 MeV was based on Geant4 simulation of the full geometry of the KBSI ECR ion source. The unfolded spectrum is overlaid by the red histogram.

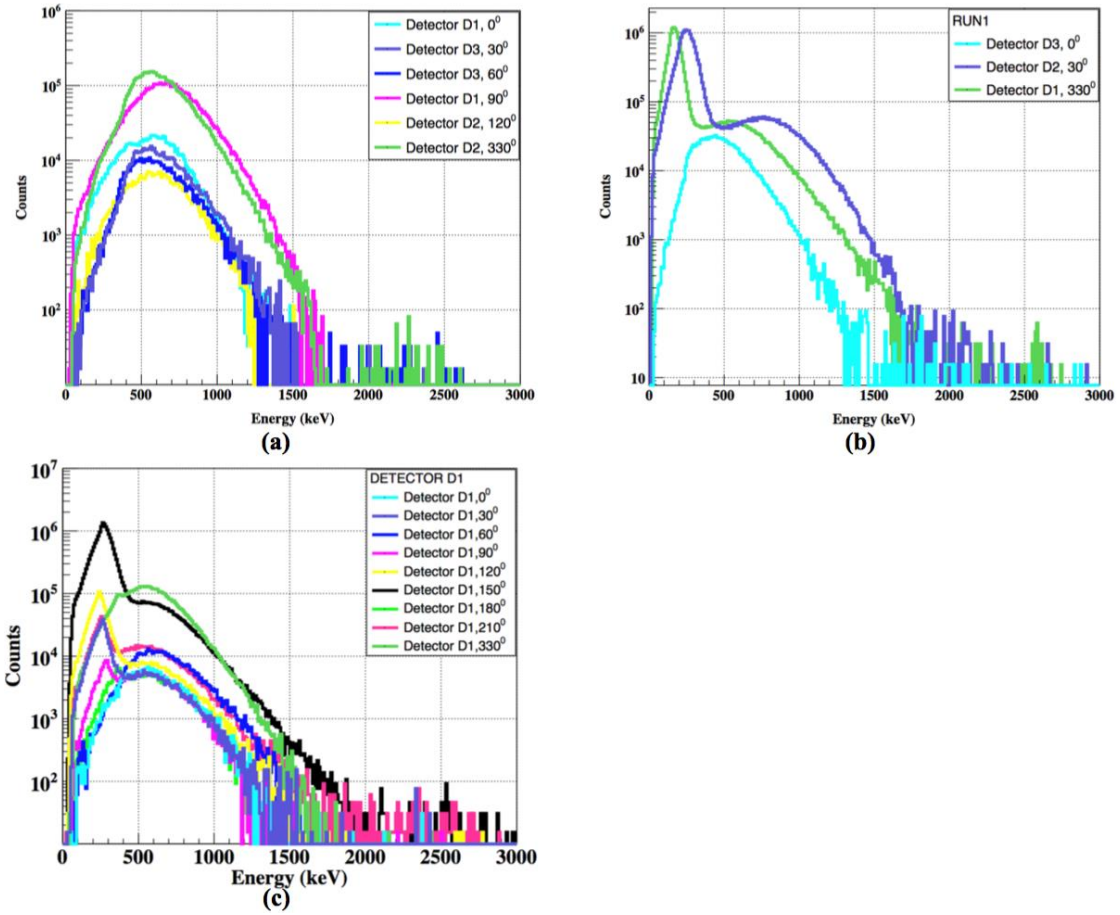

Figure 10: Measured energy spectra of the bremsstrahlung photons at the (a) injection (b) centre and (c) extraction side, respectively.

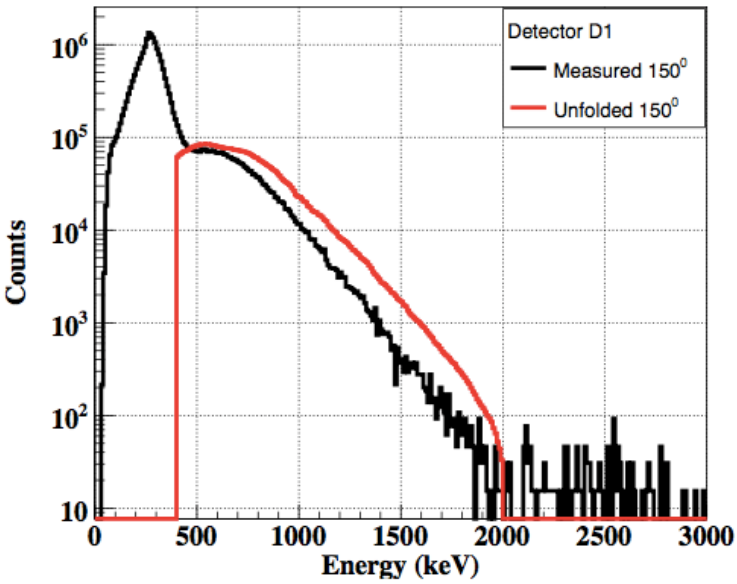

Figure 11: Unfolded energy spectra at angle 150° obtained after unfolding method.

RESULTS AND DISCUSSION

The highest end-point energy of the spectrum reaches 2.04 MeV in the radial direction as shown clearly in the unfolding spectrum (Figure 11) for angle 150° which is beyond the maximum kinetic energy available from ECR heating. The end-point energy would be approximately 1.33 MeV if the energy resolution of the NaI(Tl) detector ($\Gamma_\gamma/E_\gamma \approx 7\%$) is considered. The maximum kinetic energy (T_e) that an electron can attain from ECR heating at the cyclotron frequency $\omega = q\,B_{max}/\gamma m_e = qB_{max}\,/E_e$ is given by equation 4:

$$E_e = \frac{eB_{max}}{2\pi f}, \qquad T_e = E_e - m_e \quad (4)$$

In equation (4) m_e stand for mass of an electron, f is the microwave frequency. Here, E_e is the total energy of an electron and B_{max} denotes the maximum magnetic field strength of the ECR ion source. For $f = 28\,GHz$ and $B_{max} = 3.6\,T$, based on the ECRIS operating parameters the maximum kinetic energy is supposed to be 1.33 MeV which is inconsistent with the end-point energies observed from the experiment as clearly shown in Figure 12.

The ECR plasma was formed in the shape of a twisted triangular prism, due to the sextupole field configuration. The cross-section of the ECR plasma was a triangle at the injection side and an inverted triangle at the extraction side of the ECR ion source (Mironov *et al.*, 2015). For the injection side, the three corners of the plasma triangle correspond to angles 90°, 210° and 330°. Electrons at three corners of the triangles are accessible to hit the chamber wall and produce bremsstrahlung photons. The corners at 90° and 330° (1.68 MeV) correspond to two of the maximum angles of the plasma triangle (Figure 12(a)) while the angle at 210° was not accessible during the measurements. For the extraction side, electrons at three corners of the triangle can easily interact with the chamber wall and produce the bremsstrahlung photons. The three corners shown in Figure 12(c) of the plasma triangle correspond to the angles of 30°,150° and 270°. The last angle (270°) was not accessible due to the ECR supporting structure. The corner at 150° (2.04 MeV) corresponds to one of the maximum angles, while the second corner at 30° is off the local maximum point at 60°. The corner at angle 210° which is opposite to the maximum angle 30° by 180° to each other reaches end point energy (1.62 MeV).

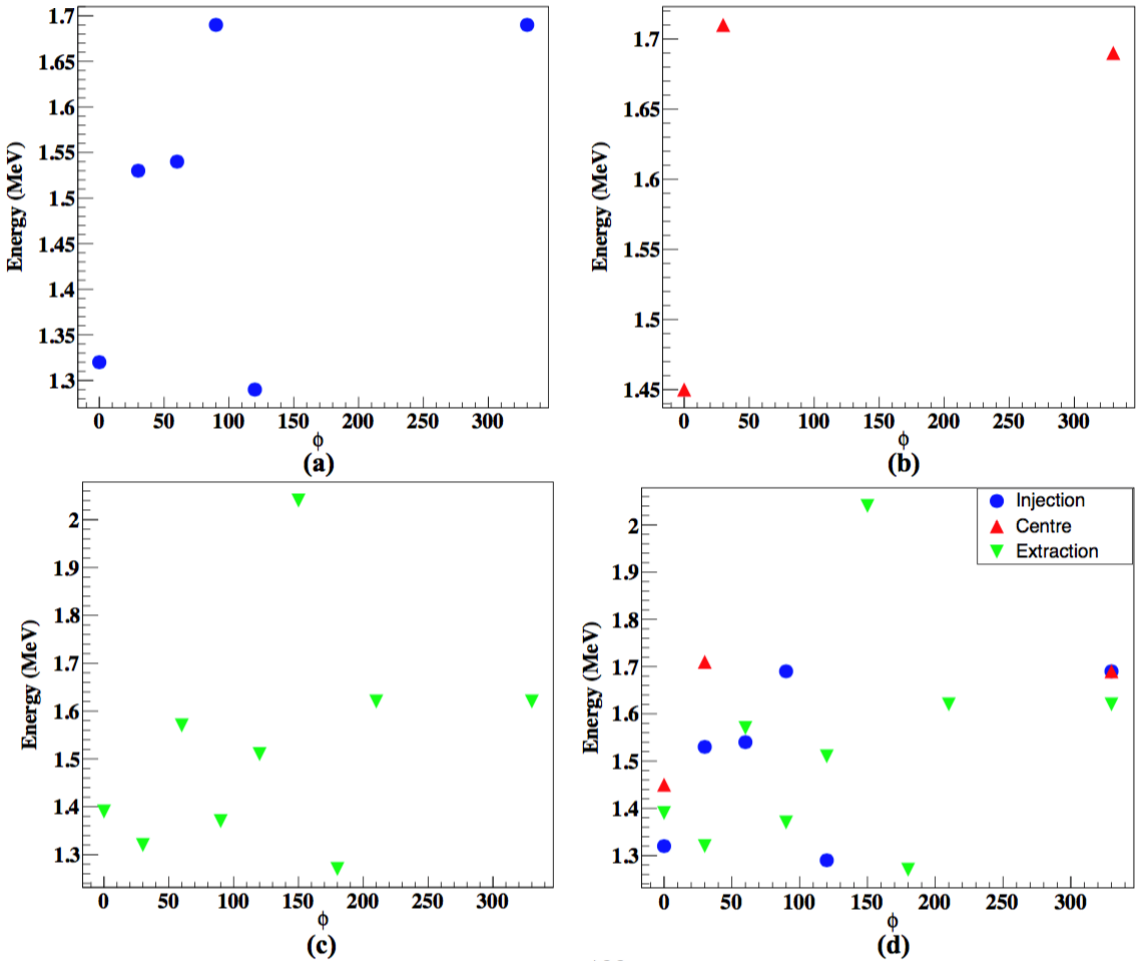

Figure 12: End-point energies distributions of the measured bremsstrahlung photons at the (a) injection (b) centre and (c) extraction side of the ECR ion source.

Furthermore, the maximum point at 210° and 330° cannot be explained by the shape of the ECR plasma. In the centre position, the ECR plasma is formed in a shape basically the same as the six-arm star (Mironov *et al.*, 2015), due to the hexapole magnetic field configuration. The six corners of the plasma shape correspond to the angles of 30°, 90°, 150°, 210°, 270° and 330°, which means after every 6 0° there should be the maximum angle. During the data measurement, three angles namely, 0° , 3 0° and 33 0° were available for measurement other angles were not accessible due to the ECR supporting structure. Electrons concentrations at two angles 30° (1.72 MeV) and 330° (1.68 MeV) of the hexagon shape at the centre position of the ECR ion source is so high and can easily collide with the chamber wall and produce the bremsstrahlung photons.

Figure 12(d) illustrates the comparison of the bremsstrahlung photons end-point energies, measured at the injection, centre and extraction sides of the ECR ion source. The distributions of the end-point energies in Figure 12(d) were represented by blue, red and green colours for the injection, centre and extraction sides respectively. Results from Figure 12(d) show that the minimum and maximum end-point energies are 1.26 MeV and 2.04 MeV at angles 18 0° and 15 0° respectively, both at the extraction side. The maximum kinetic energy of 1.33 MeV which was obtained based on the ECRIS operating parameters (using equation 4) is lower compared to the end-point energies observed from the experiment in all three-measurement locations except three angles 0° (at the

injection side) and 30° and 180° (both at the extraction side) as clearly depicted in Figure 12(c). Based on the design of this experiment, it is important to note that, the highest end-point energy values of the measured bremsstrahlung photons above the theoretical energy value of 1.33 MeV were found to be correlated with the structure of the ECR ion source and the shape of the ECR plasma in all three-measurement regions.

The results of this study were also compared with the previous studies conducted by Leitner et al., (2007) and Noland *et al.*, (2010). Results from both studies indicate greater maximum end-point energies in the radial direction than in the axial direction. Results from both Leitner, Noland and this study show that the high energy photon was most likely attributed by large number of unconfined electrons striking the chamber wall and losing their energy through the interaction with the wall material.

CONCLUSION AND RECOMMENDATION

For the first time the azimuthal angular distribution of the bremsstrahlung photons was measured at three measurement locations namely, injection, centre and extraction sides from the 28-GHz ECR ion source at the Busan center of the KBSI. The maximum end-point energies at the three measurement locations were 1.68 MeV, 1.72 MeV and 2.04 MeV for the injection, centre and extraction sides, respectively. The high end-point energy values of the bremsstrahlung photons were found to be correlated with the structure of the ECR ion source and the shape of the ECR plasma. Additionally, the high end-point energy values resulting from the bremsstrahlung photons measurements in the 28-GHz ECR plasma are due to the higher number of unconfined electrons arriving at the chamber wall easily, and producing higher bremsstrahlung photons. The unconfined electrons are the results of imperfect magnetic confinement that cause electrons to escape from the plasma volume.

ACKNOWLEDGMENTS

The authors would like to gratefully acknowledge support from the National Research Foundation of Korea and Professor Ahn of the Korea University as well as the University of Dar es Salaam.

REFERENCES

Almaz, E., and Cengiz, A. (2007). Deconvolution of Continuous Internal Bremsstrahlung Spectra of ^{32}P, ^{85}Kr and ^{143}Pr. X-RAY SPECTROMETRY, X-Ray Spectrom. 2007; **36**, 419-423.

Bhaskar, B.S., Koivisto, H., Tarvainen, O., Thuillier, T., Toivanen, V., Kalvas, T., Izotov, I., Skalyga, V., Kronholm, R., and Marttinen, M. (2021). Correlation of Bremsstrahlung and Energy Distribution of Escaping Electrons to study the Dynamics of Magnetically Confined Plasma. Plasma Physics control. Fusion 63:095010 (17pp).

Be, M. M., Chiste, V., Dulieu, C., Browne, E., Chechev, V., Kuzmenko, Helmer, R., Nichols, A., Schonfeld, E., and Dersch, R. (2004). Table of Radionuclides, 2. Monographie BIPM-5.

Benitez, J.Y., Noland, J. D., Leitner, D., Lyneis, C., Todd, D.S., and Verboncoeur, J. (2008). High Energy Component of X-ray Spectra in ECR Ion Sources. *In Proc. ECRIS'08*, Chicago, IL, USA, paper MOPO-08:77–84.

Benitez, J.Y., Lyneis, C.M., Phair, L.W., Todd, D.S., Xie, D.Z. (2016). Recent Bremsstrahlung Measurements from the Superconducting Electron Cyclotron Resonance Ion Source Venus. *Proceedings of ECRIS2016.* MOCO04.

Hajheidari, M.T., Safari, M.J., Afarideh, H., and Rouhi, H. (2016). Experimental Validation of Response Function of a NaI (Tl) Detector Modeled with Monte Carlo Codes. *Journal of Instrumentation.* 11 P06011.

Kasthurirangan, S., Agnihotri, A.N., Desai, C.A., and Tribedi, L.C., (2012).

Temperature Diagnostics of ECR Plasma by Measurement of Electron Bremsstrahlung. *Review of Scientific Instrument* **83**:073111.

Kumwenda, M.J. (2020). Deconvolution of Mono-Energetic and Multi-Lines Gamma-Ray Spectra Obtained with NaI(Tl) Scintillation Detectors Using Direct Matrix Inversion Method. Tanzania Journal of Engineering and Technology. **39**(2):104-115.

Kumwenda, M.J. (2018). Measurements of Bremsstrahlung Photons in 28-GHz Electron Cyclotron Resonance Plasma, PhD Thesis, Korea University.

Lee, B.S., Choi, S., Yoon, J.H., Park, J.Y., and Won, M.S. (2012). Manufacturing of a Superconducting Magnet System for 28-GHz Electron Cyclotron Resonance Ion Source at KBSI. *Review of Scientific Instrum*ent. **83**, 02A347.

Leitner, D., Lyneis, C.M., Loew., T., Todd, D.S., Virostek, S., and Tarvainen, O. (2006). Status Report of the 28 GHz Superconducting Electron Cyclotron Resonance Ion Source VENUS. *Review of Scientific Instrum*ent. 77:03A302.

Leitner, D., Benitez, J.Y., Lyneis, C.M., Todd, D.S., Ropponen, T., Ropponen, J., Koivisto, H., and Gammino, S. (2007). Measurement of the High Energy Component of the X-ray Spectra in the VENUS ECR Ion Source. *In Proceedings of the 12th International Conference on Ion Sources*, Jeju, Korea, August 2007.

Mironov, V., Bogomolov, S., Bondarchenko, A., Efremov, A., and Loginov, V. (2015). Numerical Model of Electron Cyclotron Resonance Ion Source. *Physics Review ST Accelerator Beams*. **18**, 123401.

Noland, J., Benitez, J.Y., Leitner, D., Lyneis, C., and Verboncoeur, J. (2010). Measurement of Radial and Axial High Energy X-ray Spectra in Electron Cyclotron Resonance Ion Source Plasmas. *Review of Scientific Instrum*ent. **81**, 02A308.

Noland, J. (2011). Measurements of Plasma Bremsstrahlung and Plasma Energy Density Produced by Electron Cyclotron Resonance Ion Source Plasmas, PhD Thesis, University of California, Berkeley.

Park, J.Y., Choi, S., Lee, B.S., Yoon, J.H., Ok, J.W., Kim, B.C., Shin, C.S., Ahn, J.K., and Won, M.S. (2014). Superconducting Magnet Performance for 28-GHz Electron Cyclotron Resonance Ion Source Developed at the Korea Basic Science Institute. *Review of Scientific Instrum*ent **85**, 02A928.

Park, J.Y., Lee, B.S., Choi, S., Kim, S.J., Ok, J.W., Yoon, J.H., Kim, H.G., Shin, C.S., Hong, J., Bahng, J., and Won, M.S. (2016). First Results of 28-GHz Superconducting Electron Cyclotron Resonance Ion Source for KBSI Accelerator. *Review of Scientific Instrum*ent. **87**: 02A717

Rahma, M.S., and Cho, G. (2010). Unfolding Low-Energy Gamma-Ray Spectrum Obtained with NaI(Tl) in Air Using Matrix Inversion Method. *Journal of Scientific Research.* **2**(2), 221-226.

Romero, E.C. (2012). Optimization of a Gas Flow Proportional Counter for Alpha Decay Measurements, Master Thesis, Universitat Munster.

Ropponen, T., Tarvainen, O., Jones, P., Peura, P., Kalvas, T., Suominen, P., Koivisto, H., and Arje, J. (2009). The Effect of Magnetic Field Strength on the Time Evolution of High Energy Bremsstrahlung Radiation Created by an Electron Cyclotron Resonance Ion Source. *Nuclear Instruments and Methods. Res., Sect.* A, 600:525-533.

Thuillier, T., Benitez, J., Biri, S., and Racz, R. (2022). X-ray Diagnostics of ECR Ion Sources Techniques, Results, and Challenges. *Review of Scientific Instrum*ent. **93**: 021102.